Antiferromagnetic Alternating and Homogeneous Manganese−Azido Chains: Structural Characterization and Magnetic Behavior of Two New One-Dimensional $[Mn(L)_2(\mu_{1,3}\text{-}N_3)_2]_n$ Compounds (L = 3-Ethylpyridine and 2-Hydroxypyridine)

Albert Escuer,*,† Ramon Vicente,† Mohamed A. S. Goher,*,‡ and Franz A. Mautner§

Departament de Química Inorgànica, Universitat de Barcelona, Diagonal 647, 08028 Barcelona, Spain, Chemistry Department, Faculty of Science, Kuwait University, P.O. Box 5969, Safat, 13060 Kuwait, and Institut für Physikalische und Theoretische Chemie, Technische Universität Graz, A-8010 Graz, Austria

Received August 13, 1997

The X-ray structures of the two monodimensional systems of formula $[Mn(L)_2(N_3)_2]_n$ in which L = 3-ethylpyridine (**1**) or 2-hydroxypyridine (**2**) have been determined. Crystal data: **1**, formula $C_{14}H_{18}MnN_8$, monoclinic $P2_1/n$, a = 10.210(5) Å, b = 15.460(6) Å, c = 10.880(4) Å, β = 95.86(3)°, Z = 4; **2**, formula $C_{10}H_{10}MnN_8O_2$, triclinic $P\bar{1}$, a = 5.218(2) Å, b = 6.841(3) Å, c = 9.469(4) Å, α = 79.30(4)°, β = 87.85(4)°, γ = 75.85(4)°, Z = 1. The two compounds consist of chains of manganese atoms bridged by double end-to-end azido bridges. **1** consists of a structurally and magnetically alternated chain whereas **2** is a homogeneous system. Magnetic measurements show antiferromagnetic interaction with J values −13.8/−11.7 and −7.0 cm^{-1} for **1** and **2**, respectively. The deformation of the $Mn_2(N_3)_2$ eight-membered rings from planarity to chair conformation has been correlated to the magnitude of the antiferromagnetic coupling constant by means of extended Hückel MO calculations.

Introduction

The results obtained in the last two years on the manganese(II)−L−azido bridged system, L = N-aromatic ligands, are surprisingly rich from both structural and magnetic points of view. The chemistry of this system is characterized by the high dimensionality of the resulting compounds (see Chart 1): 3-D for L = pyridine (py)[1,2] and 2,2′-bipyrimidine (bipym),[3,4] 2-D for the series of substituted pyridines L = 3- and 4-acetylpyridine (3-acpy[5] and 4-acpy[6]), methyl- and ethylisonicotinate (Meinc[7] and Etnic[2]), and 4-cyanopyridine (4-CNpy[5]), or 1-D for 2,2′-bipyridine.[8] A 3-D network with distorted perovskite structure was also found for $[N(CH_3)_4][Mn(N_3)_3]$.[9] In contrast, only in one case has a dinuclear compound been obtained with L = 2,2′:6′,2″-terpyridine.[10] The coordination mode of the azido bridge was found to be commonly $\mu_{1,3}$-N_3 (end-to-end), in some cases $\mu_{1,1}$-N_3 (end-on), and even alternating 1-D or 2-D systems

Chart 1

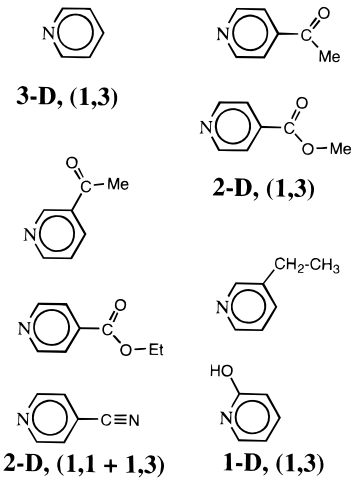

in which the two kind of coordination modes were found simultaneously in the same compound. Correlation has not been found between the properties of the L ligand and the coordination mode of the azido bridge, and from a synthetic point of view, the manganese(II)−azido system shows unpredictable behavior, analogous to that observed for copper(II) or nickel(II) azido-bridged polynuclear systems. The magnetic behavior of these compounds follows the same general trends as copper or nickel(II) systems, i.e., end-to-end azido bridges that lead to antiferromagnetic interaction and end-on bridges that give ferromagnetic coupling. The main difference in these systems is the greater dimensionality of the manganese derivatives. Systematic synthesis and magnetic study of the pyridine derivatives have recently led to the characterization of high-temperature paramagnetic behavior and low-temperature ordered phases with magnetic ordering at temperatures between 16 and

† Universitat de Barcelona (www.ub.es/inorgani/molmag.htm).
‡ Kuwait University.
§ Technische Universität Graz.

(1) Goher, M. A. S.; Mautner, F. A. *Croat. Chem. Acta* **1990**, *63*, 559.
(2) Escuer, A.; Vicente, R.; Goher, M. A. S.; Mautner, F. A. *Inorg. Chem.* **1996,** *35*, 6386.
(3) De Munno, G.; Julve, M.; Viau, G.; Lloret, F.; Faus, J.; Viterbo, D. *Angew. Chem., Int. Ed. Engl.* **1996**, *35*, 1807.
(4) Cortés, R.; Lezama, L.; Pizarro, J. L.; Arriortua, M. I.; Rojo, T. *Angew. Chem., Int. Ed. Engl.* **1996**, *35*, 1810.
(5) Escuer, A.; Vicente, R.; Mautner, F. A.; Goher, M. A. S. *Inorg. Chem.* **1997**, *36*, 3440.
(6) Escuer, A.; Vicente, R.; Goher, M. A. S.; Mautner, F. A. *Inorg. Chem.* **1995**, *34*, 5707.
(7) Escuer, A.; Vicente, R.; Goher, M. A. S.; Mautner, F. A. *J. Chem. Soc., Dalton Trans.* **1997**, 4431.
(8) Cortés, R.; Drillon, M.; Solans, X.; Lezama, L.; Rojo, T. *Inorg. Chem.* **1997**, *36*, 677.
(9) Mautner, F. A.; Cortés, R.; Lezama, L.; Rojo, T. *Angew. Chem., Int. Ed. Engl.* **1996**, *35*, 78.
(10) Cortés, R.; Pizarro, J. L.; Lezama, L.; Arriortua, M. I.; Rojo, T. *Inorg. Chem.* **1994**, *33*, 2697.

S0020-1669(97)01023-9 CCC: $15.00
Published on Web 02/05/1998

40 K for several molecular-based magnets of general formula $[Mn(L)_2(N_3)_2]$ (L = py, 3-acpy, 3-Etpy, 4-CNpy).[2,5]

Following our research on compounds of this kind, we have structurally characterized two new systems of the pyridine series, using L = 3-ethylpyridine (3-Etpy) and 2-hydroxypyridine (2-pyOH) to obtain the monodimensional systems $[Mn(3\text{-Etpy})_2(N_3)_2]_n$ (**1**) and $[Mn(2\text{-pyOH})_2(N_3)_2]_n$ (**2**). The two compounds consist of chains in which the manganese atoms are bridged by two end-to-end azido ligands showing the expected antiferromagnetic coupling. In this case, the magnetic behavior is interesting due to the distortion between the planar and the chair conformation of the $Mn_2(N_3)_2$ eight-membered rings. Correlation between the degree of distortion and the magnitude of the antiferromagnetic coupling has been successfully found by means of MO extended-Hückel calculations in a similar way to the correlation previously reported for analogous nickel(II) compounds.

Experimental Section

Synthesis. $[Mn(3\text{-Etpy})_2(N_3)_2]_n$ (**1**) was synthesized by mixing an aqueous solution (15 mL) of manganese chloride tetrahydrate (0.59 g, 3 mmol) and 1.07 g (10 mmol) of ethylpyridine dissolved in 15 mL of ethanol, followed by dropwise addition of a concentrated aqueous solution of sodium azide (0.65 g, 10 mmol). This mixture was filtered, and the resulting clear solution was left to stand in a refrigerator. After 2 weeks, white needles were formed along with a brown precipitate. The solution was filtered and the filtrate was kept in the refrigerator for some weeks, which led to the growth of X-ray suitable yellow crystals of **1**. Anal. Calcd for $MnC_{14}H_{18}N_8$: C, 47.60; H, 5.14; N, 31.72; Mn, 15.55. Found: C, 47.4; H, 5.0; N, 31.4; Mn, 15.3.

$[Mn(2\text{-pyOH})_2(N_3)_2]_n$ (**2**) was prepared in the same way as compound **1** but using the following quantities of the starting reagents: 0.79 g, 4 mmol, of manganese chloride tetrahydrate, 0.95 g, 10 mmol, of 2-hydroxypyridine, and 0.65 g, 10 mmol, of sodium azide. The resulting solution was kept in the dark in a refrigerator for *ca*. 4 months to yield large well-formed white crystals of compound **2**. Anal. Calcd for $MnC_{10}H_{10}N_8O_2$: C, 36.49; H, 3.06; N, 34.04; Mn, 16.69. Found: C, 36.3; H, 3.2; N, 33.8; Mn, 17.0.

IR Spectra. In addition to the bands of the 3-Etpy and 2-pyOH, a very strong band corresponding to the characteristic ν_{as} of the azido ligands appeared at 2072 cm^{-1} for **1** and at 2069 cm^{-1} for **2**.

Spectral and Magnetic Measurements. Infrared spectra (4000−400 cm^{-1}) were recorded from KBr pellets on a Nicolet 520 FTIR spectrophotometer. Magnetic measurements were carried out with a DSM8 pendulum susceptometer, working in the temperature range 300−4 K. The applied external magnetic field was 1.5 T. Diamagnetic corrections were estimated from Pascal tables. EPR spectra were recorded at X-band frequency with a Bruker ES200 spectrometer equipped with an Oxford liquid-helium cryostat for variable-temperature work.

X-ray Crystallography of $[Mn(3\text{-Etpy})_2(N_3)_2]_n$ (1) and $[Mn(2\text{-pyOH})_2(N_3)_2]_n$ (2). The X-ray single-crystal data for both compounds were collected on a modified STOE four-circle diffractometer. Crystal size: 0.57 × 0.50 × 0.50 mm for **1** and 0.55 × 0.35 × 0.30 mm for **2**. The crystallographic data, conditions retained for the intensity data collection, and some features of the structure refinements are listed in Table 1. Graphite-monochromatized Mo Kα radiation (λ = 0.710 69 Å) and the omega-scan technique were used to collect the data sets. The accurate unit-cell parameters were determined from automatic centering of 38 reflections (8° < θ < 15°) for **1** and 33 reflections (9.5° < θ < 19.5°) for **2** and refined by least-squares methods. A total of 4173 reflections (3458 independent reflections, R_{int} = 0.0311) were collected for **1** in the range 3.24° < θ < 27.51° and 2254 reflections (1850 independent reflections, R_{int} = 0.0230) for **2** in the range 3.12° < θ < 30.00°. Observed intensity decay of control reflections ($\bar{3}32$; 224; 062) was 9% in the case of **1** and 2% for control reflections ($\bar{1}0\bar{4}$; $22\bar{1}$) in case of **2**. Corrections were applied for Lorentz−polarization effects, for intensity decay, and for absorption using the DIFABS[11] computer program (range of transmissions: 0.279−1.000 for **1** and 0.378−1.000 for **2**). The structures were solved by direct methods, using the SHELXS-86 computer program,[12] and refined by full-matrix least-squares methods on F^2, using the SHELXL-93 computer program[13] incorporated in the SHELXTL/PC v. 5.03 program package.[14] All non-hydrogen atoms were refined anisotropically. The hydrogen atoms were obtained from ΔF maps, subsequently located on calculated positions, and assigned with isotropic displacement factors (six common ones for each type of H atom in each 3-Etpy molecule in the case of compound **1**, and five individual ones in the case of compound **2**). The final R indices were 0.0581 and 0.0356, respectively, for all observed reflections. Numbers of refined parameters were 213 (**1**) and 102 (**2**). Maximum and minimum peaks in the final difference Fourier syntheses were 0.250 and −0.232 e $Å^{-3}$ (**1**) and 0.632 and −0.736 e $Å^{-3}$ (**2**). Final atomic coordinates are reported in Tables 2 and 3, and significant bond parameters for **1** and **2** are given in Tables 4 and 5 respectively.

Table 1. Crystal Data and Structure Refinement for $[Mn(3\text{-Etpy})_2(N_3)_2]_n$ (**1**) and $[Mn(2\text{-pyOH})_2(N_3)_2]_n$ (**2**)

	1	**2**
chem formula	$C_{14}H_{18}MnN_8$	$C_{10}H_{10}MnN_8O_2$
fw	353.30	164.60
space group	$P2_1/n$	$P\bar{1}$
a, Å	10.210(5)	5.218(2)
b, Å	15.460(6)	6.841(3)
c, Å	10.880(4)	9.469(4)
α, deg	90.0	79.30(4)
β, deg	95.86(3)	87.85(4)
γ, deg	90.0	75.85(4)
V, $Å^3$	1708(1)	322.0(2)
Z	4	1
T, C	22(2)	22(2)
λ(Mo Kα), Å	0.710 69	0.710 69
d_{calc}/d_{obs}, g·cm^{-3}	1.374/1.36(2)	1.697/1.70(3)
μ(Mo Kα), mm^{-1}	0.784	1.044
R^a	0.0581	0.0356
$R^2\omega^b$	0.1161	0.0908

[a] $R(F_o) = \sum||F_o| - |F_c||/\sum|F_o|$. [b] $R_w(F_o)^2 = \{\sum[\omega(F_o)^2 - (F_c)^2)^2]/\sum[\omega(F_o)^4]\}^{1/2}$.

Results and Discussion

Description of the Structures. The two compounds show some common features, such as the *trans*-octahedral environment around the manganese atom or the 1-D arrangement obtained by means of two end-to-end azido bridges between neighboring manganese ions. However, the two chains show significant differences in the bond parameters derived from the coordination of the pyridinic ligand or the distortion from planarity of the $Mn_2(N_3)_2$ rings which may be related with the magnetic properties as discussed below.

$[Mn(3\text{-Etpy})_2(N_3)_2]_n$ (1). The labeled diagram for **1** is shown in Figure 1. The structure consists of octahedrally coordinated manganese atoms in which the coordination sites are occupied by two 3-ethylpyridine ligands in a *trans* arrangement and four azido ligands. The azido groups act as end-to-end bridging ligands with the two neighboring manganese atoms, giving a monodimensional system with double $\mu_{1,3}$ bridges along the [001] direction, Figure 2. Inversion centers, placed between the manganese atoms but not on the manganese atoms, allow an alternating chain. As a consequence, the bond parameters

(11) Walker, N.; Stuart, D. *Acta Crystallogr.* **1983**, *A39*, 158.
(12) Sheldrick, G. M. *SHELXS-86, Program for the Solution of Crystal Structures*; University of Gottingen: Germany, 1986.
(13) Sheldrick, G. M. *SHELXL-93, Program for the Refinement of Crystal Structures*; University of Gottingen: Germany, 1993.
(14) *SHELXTL 5.03 (PC-Version), Program Library for the Solution and Molecular Graphics*; Siemens Analytical Instruments Division: Madison, WI, 1995.

Table 2. Atomic Coordinates ($\times 10^4$) and Equivalent Isotropic Displacement Parameters ($Å^2 \times 10^3$) for $[Mn(3\text{-Etpy})_2(N_3)_2]_n$ (**1**)

atom	*x*	*y*	*z*	*U*(eq)[a]
Mn(1)	9(1)	4981(1)	2490(1)	45(1)
N(11)	1441(3)	5375(3)	1174(3)	69(1)
N(12)	1458(3)	5338(2)	116(3)	42(1)
N(13)	1511(3)	5300(2)	−942(3)	60(1)
N(21)	1547(3)	5240(2)	4066(3)	56(1)
N(22)	1437(3)	5319(2)	5118(3)	40(1)
N(23)	1395(3)	5410(2)	6169(3)	64(1)
N(1)	784(3)	3602(2)	2388(3)	56(1)
C(1)	49(4)	2971(3)	1867(4)	64(1)
C(2)	477(5)	2127(3)	1733(4)	77(1)
C(3)	1749(5)	1948(3)	2183(4)	74(1)
C(4)	2526(4)	2591(3)	2733(5)	80(1)
C(5)	2009(4)	3403(3)	2813(4)	73(1)
C(6)	−448(7)	1455(3)	1084(8)	147(3)
C(7)	−427(8)	685(5)	1495(10)	229(5)
N(2)	−693(3)	6382(2)	2521(3)	54(1)
C(8)	−526(4)	6880(3)	3535(4)	59(1)
C(9)	−871(4)	7739(3)	3585(4)	63(1)
C(10)	−1469(4)	8101(3)	2529(5)	72(1)
C(11)	−1666(4)	7609(3)	1476(4)	75(1)
C(12)	−1254(4)	6766(3)	1506(4)	68(1)
C(13)	−530(6)	8271(3)	4744(4)	91(2)
C(14)	573(8)	8876(5)	4635(6)	156(3)

[a] *U*(eq) is defined as one-third of the trace of the orthogonalized $\mathbf{U}_{ij}$ tensor.

Table 3. Atomic Coordinates ($\times 10^4$) and Equivalent Isotropic Displacement Parameters ($Å^2 \times 10^3$) for $[Mn(2\text{-pyOH})_2(N_3)_2]_n$ (**2**)[a]

atom	*x*	*y*	*z*	*U*(eq)[a]
Mn(1)	0	0	0	24(1)
N(11)	3026(3)	−749(3)	1775(2)	34(1)
N(12)	5291(3)	−1296(2)	1573(1)	25(1)
N(13)	2431(3)	1866(3)	−1405(2)	38(1)
O(1)	2339(3)	−2782(2)	−688(1)	33(1)
C(1)	3531(3)	−2928(2)	−1868(2)	26(1)
C(2)	2519(3)	−1850(3)	−3239(2)	33(1)
C(3)	3984(4)	−2093(3)	−4439(2)	39(1)
C(4)	6531(4)	−3404(3)	−4345(2)	42(1)
C(5)	7454(4)	−4467(3)	−3039(2)	38(1)
N(1)	5971(3)	−4225(2)	−1850(2)	30(1)

[a] *U*(eq) is defined as one-third of the trace of the orthogonalized $\mathbf{U}_{ij}$ tensor.

Table 4. Selected Bond Lengths (Å) and Angles (deg) for $[Mn(3\text{-Etpy})_2(N_3)_2]_n$ (**1**)

Manganese Environment			
Mn(1)−N(13A)	2.214(3)	Mn(1)−N(21)	2.240(3)
Mn(1)−N(23B)	2.230(3)	Mn(1)−N(1)	2.280(3)
Mn(1)−N(11)	2.234(3)	Mn(1)−N(2)	2.284(3)
Azido Bridges			
N(11)−N(12)	1.154(4)	N(21)−N(22)	1.168(4)
N(12)−N(13)	1.159(4)	N(22)−N(23)	1.157(4)

N(1)−Mn(1)−N(2)	177.0(1)	N(11)−Mn(1)−N(23B)	179.0(1)
N(1)−Mn(1)−N(11)	88.3(1)	N(13A)−Mn(1)−N(21)	179.0(1)
N(1)−Mn(1)−N(13A)	90.0(1)	N(13A)−Mn(1)−N(23B)	89.9(1)
N(1)−Mn(1)−N(21)	89.1(1)	N(21)−Mn(1)−N(23B)	89.7(1)
N(1)−Mn(1)−N(23B)	91.6(1)	N(12)−N(11)−Mn(1)	134.7(3)
N(2)−Mn(1)−N(11)	88.7(1)	N(12)−N(13)−Mn(1A)	131.8(3)
N(2)−Mn(1)−N(13A)	90.0(1)	N(22)−N(21)−Mn(1)	129.7(3)
N(2)−Mn(1)−N(21)	90.9(1)	N(22)−N(23)−Mn(1B)	134.8(3)
N(2)−Mn(1)−N(23B)	91.4(1)	N(21)−N(22)−N(23)	176.5(4)
N(11)−Mn(1)−N(13A)	91.1(1)	N(11)−N(12)−N(13)	178.3(4)
N(11)−Mn(1)−N(21)	89.3(1)	N(11)−Mn(1)−N(23B)	179.0(1)

in the bridging region between Mn(1) and Mn(1A) and Mn(1) are different: Bond lengths are Mn(1)−N(11) = 2.234(3) Å and Mn(1)−N(13A) = 2.214(3) Å *vs* Mn(1)−N(21) = 2.240(3) Å and Mn(1)−N(23B) = 2.230(3) Å, and bond angles are

Table 5. Selected Bond Lengths (Å) and Angles (deg) for $[Mn(2\text{-pyOH})_2(N_3)_2]_n$ (**2**)

Manganese Environment			
Mn(1)−O(1)	2.191(2)	N(12)−N(13A)	1.171(2)
Mn(1)−N(13)	2.245(2)	N(1)−O(1B)	2.863(2)
Mn(1)−N(11)	2.250(2)	H(5)−O(1B)	2.029(2)
N(11)−N(12)	1.169(2)	N(1)−H(5)	0.86

O(1)−Mn(1)−N(11)	85.04(7)	N(11)−Mn(1)−N(13C)	89.69(7)
O(1)−Mn(1)−N(13)	90.00(7)	N(12)−N(11)−Mn(1)	122.3(1)
O(1C)−Mn(1)−N(11)	94.96(7)	N(12A)−N(13)−Mn(1)	123.8(1)
O(1C)−Mn(1)−N(13)	90.00(7)	N(11)−N(12)−N(13A)	178.4(2)
N(11)−Mn(1)−N(13)	90.31(7)	N(1)−H(5)−O(1B)	165.3(1)

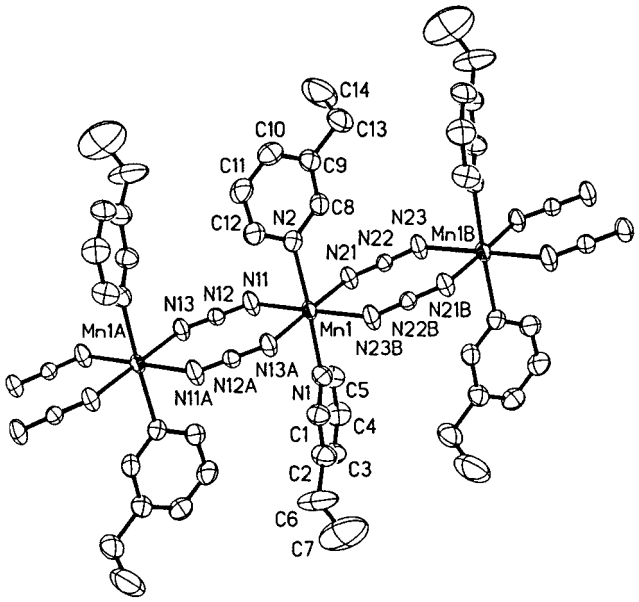

Figure 1. ORTEP drawing (50% thermal ellipsoid probability) of $[Mn(3\text{-Etpy})_2(N_3)_2]_n$ (**1**) with the atom-labeling scheme.

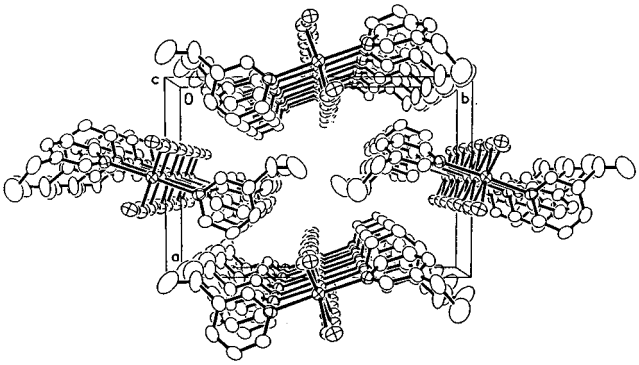

Figure 2. View of the unit cell of $[Mn(3\text{-Etpy})_2(N_3)_2]_n$ (**1**) showing the well-isolated chains along the [001] axis.

Mn(1)−N(11)−N(12) =134.7(3)° and Mn(1)−N(13A)−N(12A) = 131.8(3)° *vs* Mn(1)−N(21)−N(22) = 129.7(3)° and Mn(1)−N(23B)−N(22B) = 134.8(3)°. The Mn(1)−Mn(1A) = 5.418(3) Å distance is also slightly shorter than Mn(1)−Mn(1B) = 5.463(3) Å. The distortion of the $Mn_2(N_3)_2$ ring from planarity to chair conformation is also greater for the Mn(1)−$(N_3)_2$−Mn(1B) (ring 2) than for Mn(1)−$(N_3)_2$−Mn(1A) (ring 1). The degree of distortion may be quantified by means of the δ acute angle between the normal to the planes defined by the six N atoms of the azido bridges and the corresponding N−Mn−N planes: δ for ring 1 is 6.9(2)° (torsion Mn(1)−N(11)−N(12)−N(13)−Mn(1A) 13.5(4)°) whereas δ for ring 2 is 11.6(2)° (torsion Mn(1)−N(21)−N(22)−N(23)−Mn(1B) 23.2(3)°). The

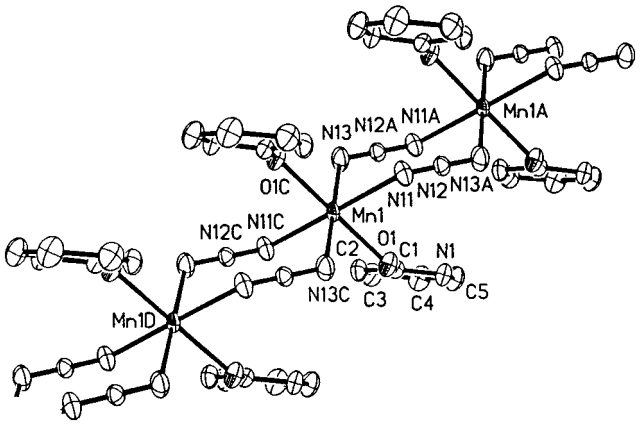

Figure 3. ORTEP drawing (50% thermal ellipsoid probability) of $[Mn(2\text{-pyOH})_2(N_3)_2]_n$ (**2**) with the atom-labeling scheme.

neutral chains of $[Mn(3\text{-Etpy})_2(N_3)_2]_n$ (**1**) are well isolated by the 3-ethylpyridine ligands, the minimum Mn−Mn interchain distance being 9.253(5) Å.

$[Mn(2\text{-pyOH})_2(N_3)_2]_n$ (2). The labeled diagram for **2** is shown in Figure 3. In this case there is an inversion center on the manganese atoms and also between the manganese atoms, giving a 1-D homogeneous system along [100] direction. Axial bond lengths Mn(1)−O(1) = 2.191(2) Å, are shorter than the Mn(1)−N(11) and Mn(1)−N(13) = 2.250(2) and 2.245(2) Å respectively. Manganese−azido bonds angles are similar, Mn(1)−N(11)−N(12) = 122.3(1)° and Mn(1)−N(13)−N(12A) = 123.8(1)° but lower than compound **1** due to the larger chair distortion of the $Mn_2(N_3)_2$ ring. For **2**, the δ parameter takes the 38.0° value (torsion Mn(1)−N(11)−N(12)−N(13A)−Mn(1A) 63.1(2)°) and the manganese atoms are displaced 0.976 Å from the plane defined by the six N atoms. $[Mn(2\text{-pyOH})_2(N_3)_2]_n$ shows an interesting feature related to the pyridinic ligand: Coordination to the manganese atom is done by means of the oxygen instead of the nitrogen donor as occurs in the remaining compounds of this $[Mn(R\text{-pyridine})_2(N_3)_2]_n$ series characterized to date. The H(5) atom is placed on the nitrogen, and then the ligands may be described as the tautomeric form of 2-hydroxypyridine. A network of interchain hydrogen bonds was found involving O(1), N(1), and H(5) of neighboring chains: N(1)−O(1B) is 2.863(2) Å, and the overall structure may be described as sheets of $[Mn(2\text{-pyOH})_2(N_3)_2]_n$ chains closely related by a network of hydrogen bonds, Figure 4.

Magnetic Data. The $\chi_M T$ product and the molar magnetic susceptibilities *vs* T in the 300−4 K range of $[Mn(3\text{-Etpy})_2(N_3)_2]_n$ (**1**) and $[Mn(2\text{-pyOH})_2(N_3)_2]_n$ (**2**) are plotted in Figure 5. The overall behavior of **1** corresponds to an antiferromagnetically coupled system, as expected from the structural data. The $\chi_M T$ value decreases on cooling from 2.96 $cm^3 \cdot K \cdot mol^{-1}$ at 290 K and tends to zero at low temperature, showing a maximum of susceptibility at 80 K. Strictly, compound **1** is a one-dimensional alternating Heisenberg antiferromagnet, which may be analyzed by means of the expression[8] derived from the Hamiltonian $H = -J_1\sum S_{2i}S_{2i+1} - J_2 S_{2i}S_{2i+2}$. Best fit parameters were $J_1 = -13.8(2)$ cm^{-1}, $J_2 = -11.7(2)$ cm^{-1}, and $g = 1.99$.

For **2** the $\chi_M T$ value decreases on cooling from 3.66 $cm^3 \cdot K \cdot mol^{-1}$ at 290 K and tends to zero at low temperature, showing a maximum of susceptibility at 50 K. The fit for the homogeneous chain **2** was performed with the analytical expression[15] derived by Fisher for the magnetic susceptibility

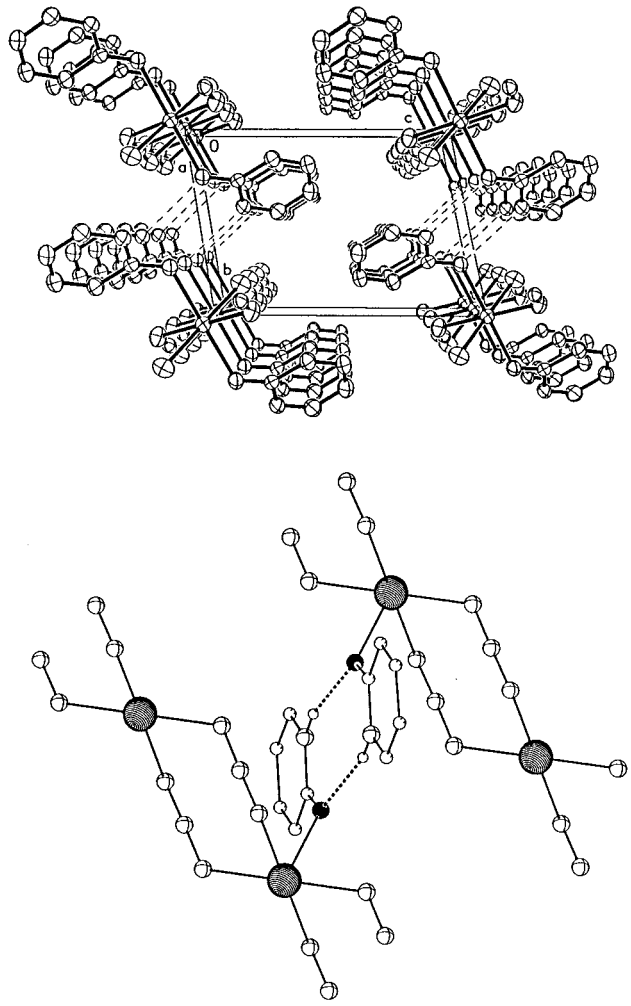

Figure 4. Top: View of the unit cell of $[Mn(2\text{-pyOH})_2(N_3)_2]_n$ (**2**) showing the chains along the [100] axis related by the hydrogen bonds between N(1) and O(1) of different chains. Bottom: Details of the double hydrogen bond between the neighboring hydroxopyridine groups.

of an infinite chain of classical spins based on the Hamiltonian $H = -J\sum S_i S_{i+1}$ for local spin values $S = {}^5/_2$. The best fit parameters are J = −7.0(1) cm^{-1} and $g = 2.03$, Figure 5.

EPR spectra at room temperature show sharp isotropic signals centered at $g = 2.0$. The peak-to-peak line width increases at low temperature maintaining the $g = 2.0$ value down to 4 K.

Magneto−Structural Correlations. The title compounds permit the comparable experimental study of the effect of the changes in the bond parameters *vs* the superexchange J value, since the two compounds show the same dimensionality (1−D), have the same kind of bridge (two end-to-end azido bridging ligands) and, in addition, show the same arrangement around the manganese atom (two pyridinic ligands in *trans*-octahedral coordination). This kind of correlation has been performed successfully for singly[16] and doubly[17,18] end-to-end nickel(II) azido-bridged complexes (d^8, e_g atomic orbitals involved in the superexchange pathway), for which a large number of chains and dinuclear compounds confirm that the antiferromagnetic component of the superexchange J value is strongly dependent

(15) Fisher, M. E. *Am. J. Phys.* **1964**, *32*, 343.

(16) Vicente, R.; Ribas, J.; El Fallah, M. S.; Solans, X.; Font-Bardia, M. *Inorg. Chem.* **1994**, *33*, 1842.

(17) Ribas, J.; Monfort, M.; Bastos, C.; Diaz, C.; Solans, X. *Inorg. Chem.* **1993**, *32*, 3557.

(18) Vicente, R.; Escuer, A. *Polyhedron* **1995**, *14*, 2133.

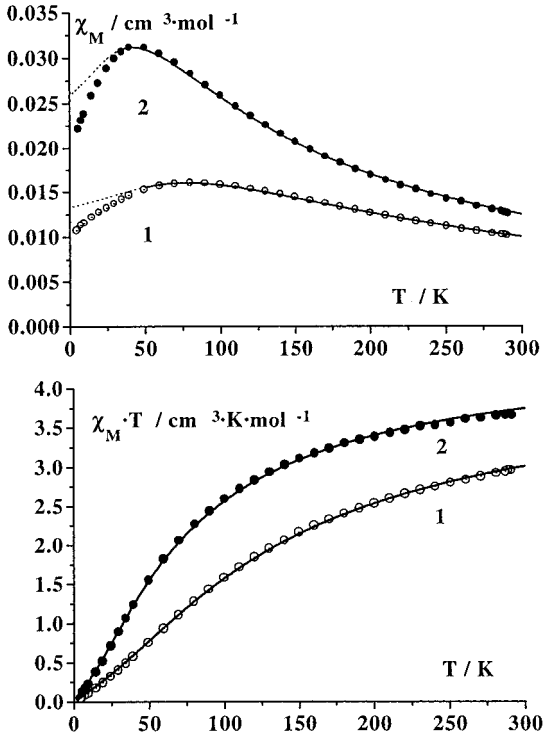

Figure 5. χ_M *vs T* (top) and $\chi_M T$ *vs* T (bottom) plots for compounds **1** and **2**. The solid line shows the best fit theoretical curve. Dashed curves correspond to the theoretical plot below the lower range of temperature used to fit the experimental data.

on the bond angles in the bridging region. Recently[2,8] this kind of correlation has been extended to the manganese(II) ion on the basis of two structural τ (strictly defined as the angle between the mean planes Mn−N(1)−N(2)−N(3) and N(1)−N(2)−N(3)−Mn′) or δ (defined as the dihedral angle between the plane defined for the six N-azido atoms and the N(1)−Mn−N(3′) plane) parameters:

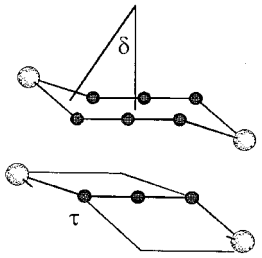

As occurs for d^8 ions, for singly d^5 azido-bridged compounds it was shown[2] that the antiferromagnetic interaction should decrease for large Mn−N−N bond angles and large Mn−N_3−Mn torsion angles. The τ parameter may also be used for doubly azido-bridged compounds, but the most useful parameter is the dihedral δ angle: increase of δ implies simultaneously decrease in Mn−N−N bond angles and larger τ torsion.

To study the relation between δ and the superexchange *J* parameter, the Hay−Thibeault−Hoffmann relationship[20] between the $\Sigma\Delta^2$ and the antiferromagnetic contribution to the antiferromagnetic contribution of *J* is useful. Δ values (difference of energy between MOs of the same symmetry) may be easily obtained by means of MO extended Hückel calculations.

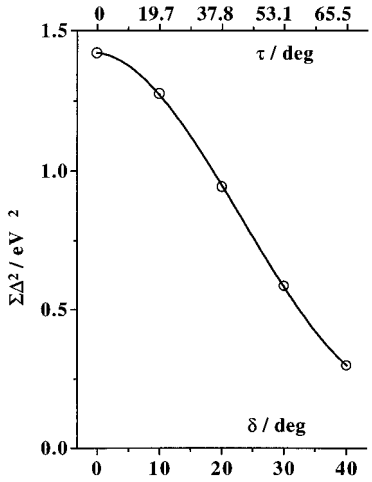

Figure 6. Variation of $\Sigma\Delta^2$ as a function of the dihedral angle δ or the equivalent parameter torsion τ.

Table 6. Main Structural and Magnetic Parameters for the Mn−($\mu_{1,3}$-N_3)−Mn Rings Characterized to Date, Showing the Relationship between *J* and τ or δ

compd	Mn−N−N (deg)	Mn[a] (Å)	τ (deg)	δ (deg)	*J* (cm^{-1})	ref
$[Mn(bipy)(N_3)_2]$	131.1 127.3	0.601	41.1	22.7	−11.9	8
$[Mn(3\text{-}Etpy)_2(N_3)_2]$	134.7 131.7	0.187	13.5	6.9	−11.7	this work
	134.8 129.7	0.320	23.2	11.6	−13.8	this work
$[Mn(pyOH)_2(N_3)_2]$	123.8 122.4	0.976	63.1	38.0	−7.0	this work

[a] Mn corresponds to the distance between the manganese atom and the plane defined by the six N atoms of the bridges.

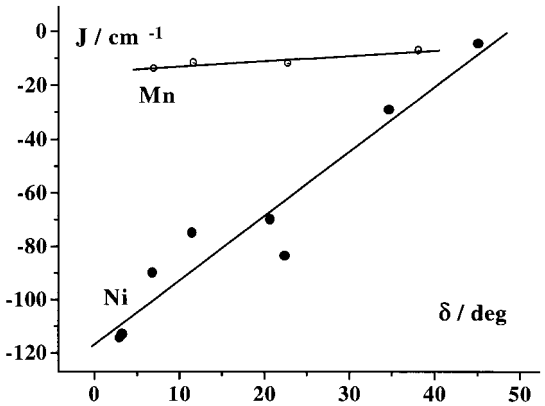

Figure 7. Plot of the experimental *J* values vs the dihedral angle δ for several nickel dinuclear complexes and the available data for manganese systems with double end-to-end azido bridges, showing the correlation between these parameters both for d^8 and d^5 ions.

The CACAO program[19] was used on the $[(NH_3)_4Mn-(N_3)_2-Mn(NH_3)_4]^{2+}$ model varying the δ parameter within the experimental limits found to date (δ = 0°/40° or equivalently the Mn−N_3−Mn′ torsion τ = 0°/65°).

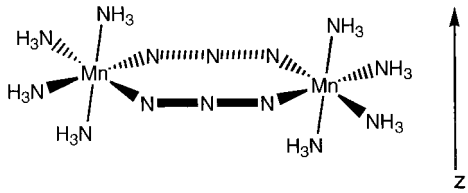

(19) Mealli, C.; Proserpio, D. M. CACAO program (Computed Aided Composition of Atomic Orbitals). *J. Chem. Educ.* **1990**, *67*, 399.
(20) Hay, P. J.; Thibeault, J. C.; Hoffmann, R. *J. Am. Chem. Soc.* **1975**, *97*, 4884.

The results of the calculations, as $\Sigma\Delta^2$ *vs* δ or τ, are plotted in Figure 6, showing the expected similar behavior between d^8 and d^5 ions: Antiferromagnetic coupling should decrease for larger δ values, indicating that the loss of overlap due to the increase in the torsion angles (implicit with the increase in δ) becomes the driving force that controls the antiferromagnetic coupling.

This result agree with the experimental *J* values obtained for the three compounds with bridges of this kind synthesized to date, $[Mn(bipy)(N_3)_2]_n$, $[Mn(3\text{-}Etpy)(N_3)_2]_n$, and $[Mn(2\text{-}pyOH)(N_3)_2]_n$, as is summarized in Table 6.

Comparison with the [NiNi] pairs with a double-azido bridge shows the general validity of the proposed dependence of the experimental *J* value on δ, Figure 7. For the two ions, *J* decreases strongly for lower values of δ, this variation being more drastic for nickel systems. One possible explanation may be related with the different superexchange pathways: For nickel(II), d^8, the only pathway is derived from the d_{z^2} atomic orbitals of the nickel atoms, and loss of overlap due to the increase in δ led to a rapid fall in *J* values. For manganese(II), d^5, the main superexchange pathway is the same as a d^8 ion, but also there is some contribution of the t_{2g} atomic orbitals which allows a smooth decrease of *J*, as was recently proposed for the single-azido system.

Acknowledgment. A.E. and R.V. thank the CICYT (Grant PB093/0772) for support of this research. F.A.M. thanks Prof. C. Kratky and Dr. F. Belaj (University of Graz) for the use of experimental equipment.

Supporting Information Available: Complete listings of full data collection and processing parameters, bond lengths and bond angles, atomic coordinates, anisotropic displacement coefficients, and hydrogen atom coordinates (16 pages). Ordering information is given on any current masthead page.

IC971023Q